Exchange-coupled Fe-Pt/Ru/Fe-Pt nanogranular films as potential HAMR media with reduced writing temperature

Daisuke Ogawa,[1,*] Anton Bolyachkin,[1] Angayarkanni R. Dilipan,[1,2] Nikita Kulesh,[1] Hossein Sepehri-Amin,[1,2] and Yukiko K. Takahashi[1,†]

[1] *National Institute for Materials Science, Tsukuba 305-0047, Japan*
[2] *Graduate School of Science and Technology, University of Tsukuba, Tsukuba 305-8577, Japan*

Heat-assisted magnetic recording (HAMR) is a promising high-density data storage technology whose intensive practical deployment requires a perfect balance of many factors, including device reliability, which is challenged by severe writing conditions. In this work, we propose HAMR media composed of Fe-Pt/Ru/Fe-Pt trilayer nanograins embedded into a carbon segregating matrix. When the Ru nonmagnetic spacer is thinner than 2 nm, the Fe-Pt layers were found to be exchange-coupled and exhibit different Curie temperatures, which is beneficial for lowering the HAMR writing temperature. Given the grain size of 17 nm, sufficient thermal stability was preserved according to the time dependence of coercivity analyzed using the Sharrock equation. The granular microstructure of Fe-Pt/Ru/Fe-Pt films with different Ru thicknesses was examined in detail, while their magnetic properties were interpreted by micromagnetic simulations distinguishing the properties of individual Fe-Pt layers. Grain size reduction, suppression of in-plane variants, improvement of the degree of $L1_0$ order in the top Fe-Pt layer - all these are further steps to optimize the developed exchange-coupled Fe-Pt/Ru/Fe-Pt nanogranular films, that would open a new avenue for tuning the HAMR media toward its ultimate performance.

Keywords: heat-assisted magnetic recording, exchange-coupled media, Fe-Pt, Curie temperature

I. INTRODUCTION

In the epoch of digital transformation, the amount of data being accumulated and handled globally is growing exponentially. As a result, increasing the storage capacity of data centers has emerged as a critical issue. Data centers mainly utilize hard disk drives (HDDs) owing to their substantial capacity, non-volatility, and low bit cost. The current recording density in commercial HDDs is about 1.5 Tbit/in^2. This is achieved with a conventional perpendicular magnetic recording media – a granular media with ferromagnetic Co-Cr-Pt grains uniformly dispersed in a SiO_2-based nonmagnetic matrix. The next generation ultra-high-density HDDs are under development and are expected to exceed 4 Tbit/in^2 in response to societal demands [1, 2].

Achieving a recording density over 4 Tbit/in^2 requires reducing the grain size to 5 nm or less. The conventional Co-Cr-Pt recording media cannot withstand that without violating the thermal stability condition: $K_uV/k_BT > 60$, where K_u is the uniaxial magnetocrystalline anisotropy constant, V is the volume of a grain, k_B is the Boltzmann constant, and T is the temperature [3]. $L1_0$-ordered FePt can overcome this problem due to its high K_u of 7 MJ/m^3 [4] that theoretically ensures thermal stability down to 4 nm grain size [5]. However, such a strong magnetic anisotropy leads to another challenge - an external magnetic field larger than 3 T is necessary to switch FePt grains at room temperature, exceeding the 1.5 T capability of standard recording heads [6]. An energy-assisted magnetic recording (EAMR) has been proposed, which essential idea is to stimulate the magnetization reversal by applying external energy such as heat and/or microwaves. The former, heat-assisted magnetic recording (HAMR) [6], appears to be the most feasible option with first HAMR HDDs deployed in 2020. However, there are still several issues on the way to the desired ultra-high recording density and mass production. One is the low reliability of the HAMR HDD, which is attributed to writing at elevated temperatures approaching the Curie temperature (T_c) of FePt around 760 K [7, 8]. Even a few nanoseconds of such intense heating may cause deformations in both the recording media and writing head [9, 10]. Furthermore, lubricants protecting the surface of the medium are also prone to degrade with heat exposure [11].

To address these issues, reducing the T_c of FePt media can be considered to lower the writing temperature. This can be achieved by doping FePt with Ni [12], Mn [13], or Ru [14, 15]. However, such doping has inherent limitations as it significantly reduces the magnetic anisotropy and saturation magnetization, M_s, thus affecting K_uV/k_BT and the signal-to-noise ratio. Exchange-coupled composite (ECC) can inspire to a more adjustable solution which could be less detrimental to M_s and effective K_u. For the ECC media, originally proposed as granular media with stacked high anisotropy and soft magnetic layers, a well-tunable switching field with maintained thermal stability was demonstrated [16–22]. This concept can be adapted to HAMR media: nanograins are split into exchange-coupled high- and low-T_c FePt layers to adjust the writing temperature of the media, while preserving sufficient K_uV/k_BT (see Fig. 1 for a schematic explanation). Other potential benefits

* ogawa.daisuke@nims.go.jp
† takahashi.yukiko@nims.go.jp

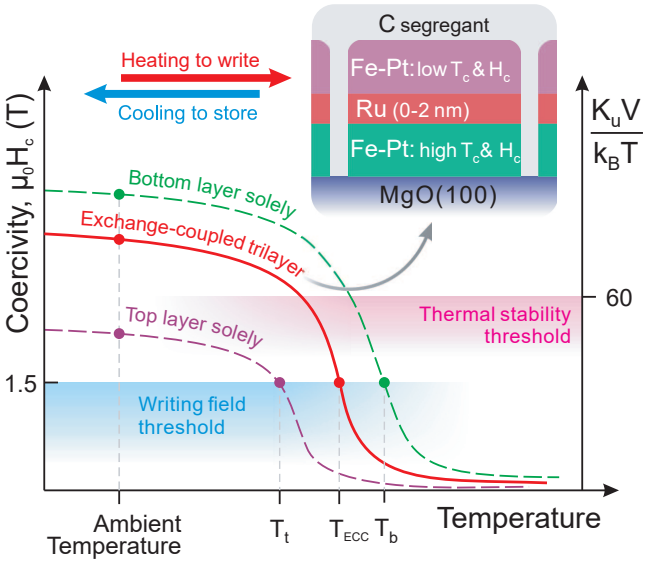

FIG. 1. The schematic temperature dependencies of coercivity (H_c) and normalized energy barrier (K_uV/k_BT) for the individual Fe-Pt layers and the entire Fe-Pt/Ru/Fe-Pt granular stack (inset). Although K_uV/k_BT is expected to decrease more steeply than H_c with increasing temperature, both are represented by one curve for simplicity.

of ECC-HAMR in different realizations include reduced thermal write errors [23–25], improved switching probability [26], increased near-field transducer lifespan [27], and suppressed transition jitter noise [28].

In this work, exchange-coupled HAMR granular media was developed by depositing Fe-Pt/Ru/Fe-Pt trilayer structure with C as a segregant (Fig. 1, inset). The measured hysteresis loops of the films were interpreted with micromagnetic simulations, which clearly indicated exchange coupling of the Fe-Pt layers when the Ru spacer was thin enough, while temperature dependencies of magnetization revealed the difference in Curie temperatures. The appropriate thermal stability of the developed films was confirmed by the time dependence of the coercivity. Thus, the practical feasibility of the ECC-HAMR media has been demonstrated. With further microstructural optimization, it will contribute to the realization of robust high-density HAMR media.

II. EXPERIMENTAL DETAILS

The nanogranular films were fabricated using an ultrahigh vacuum magnetron sputtering system with a base pressure around 10^{-7} Pa. All films were deposited on a single crystal MgO(100) substrate to promote the (001) textured growth of Fe-Pt with $L1_0$ chemical order [15, 29–31]. The nominal film stack was composed of Fe-Pt(4.5)/Ru(0-2.0)/Fe-Pt(4.5) with 20 vol.% of C as a segregant in each layer. Both the top and bottom Fe-Pt layers of 4.5 nm thickness were deposited by co-sputtering Fe-Pt and C targets at 500 °C under Ar pressure of 0.478 Pa. The Ru layer, also called the spacer, was deposited under the same conditions using Ru and C targets; its thickness was varied from 0 (no spacer) to 2 nm. To prevent from oxidation, a 5 nm thick C capping layer was deposited at room temperature. For simplicity, the described films are referred to as Fe-Pt/Ru(t_{sp})/Fe-Pt hereinafter with t_{sp} representing the thickness of the Ru spacer in nm.

X-ray diffraction (XRD) was used to evaluate the crystal structure and degree of the $L1_0$ order (S) using a Rigaku SmartLab with a Cu-Kα X-ray source. S was evaluated following the equation [32–34]:

$$S = \sqrt{\frac{I_{001}}{I_{002}} \times \frac{(|F|^2LPAD)_{002}}{(|F|^2LPAD)_{001}}} = \alpha\sqrt{\frac{I_{001}}{I_{002}}}, \qquad (1)$$

where I_{001} and I_{002} are experimental integrated intensities of the $L1_0$ (001) superlattice and (002) fundamental peaks, respectively. F, L, P, A, and D are the structure factor, Lorentz factor, polarization factor, absorption factor, and temperature factor, respectively – all are used to calculate theoretical (001) and (002) integrated peak intensities assuming perfect out-of-plane (001) texture of the Fe-Pt grains. The coefficient α stands for the processed ratio of theoretical intensities and depends on the experimental setup, in our case $\alpha = 0.85$ [35–37].

The top view and cross-sectional transmission electron microscopy (TEM) of the films was performed using a Titan G2 80-200 with a probe aberration corrector. Electron-transparent samples for these TEM observations were prepared using chemical etching and a lift-out technique using a focused ion beam (FEI Helios Nanolab 650), respectively. To prevent damage during ion beam milling, the films were coated with Ni. Energy-dispersive X-ray spectroscopy (EDS) was carried out using a FEI Super-X EDX detector, while the results were analyzed using the Bruker Esprit v1.9 software. The local crystal structure was examined via selected area electron diffraction (SAED) using TEM. Statistical analysis of the granular microstructure in the top view TEM images was performed using deep learning models [38].

Out-of-plane (OOP) hysteresis loops were measured using a superconducting quantum interference device (SQUID) magnetometer (Quantum Design) in magnetic fields up to 7 T over the temperature range from 100 to 700 K. Measurements of the in-plane (IP) hysteresis loops were carried out using a Dynacool PPMS (Quantum Design) with 14 T maximum magnetic field, which was equipped with a large bore coil set. Curie temperatures (T_c) were determined by fitting the M-T curves using the Kuz'min formula [39].

To analyze the OOP demagnetization curves, micromagnetic simulations were performed by solving the Landau–Lifshitz–Gilbert equation with unit damping constant and sweeping rate of 0.4 T/ns via the Fastmag software [40]. Finite element models of nanogranular Fe-Pt

films with the trilayer structure were developed following a similar approach to that in Refs. [15, 41].

III. RESULTS AND DISCUSSION

A. Microstructure

The reference Fe-Pt film devoid of a Ru spacer (t_{sp} = 0 nm) exhibited a fine granular microstructure with the mean grain size (D) of 17.5 nm and the number density of 1.43 Tgrain/in^2 (Fig. 2(a)). The introduction of a thin Ru(0.5) spacer did not alter the top view microstructure much, preserving the grain size and number density at 17.6 nm and 1.48 Tgrain/in^2, respectively (Fig. 2(b)). These parameters deteriorated to 19.3 nm and 1.23 Tgrain/in^2 as the Ru thickness increased to 1.0 nm (Fig. 2(c)). This was accompanied by a tendency to grain coalescence, which finally resulted in a network-like structure when the Ru spacer approached 2 nm in thickness, as shown in Fig. 2(d). For all films, the SAED patterns revealed (110) superlattice spots indicative of $L1_0$ Fe-Pt, along with (020) and (022) fundamental spots. The (020) diffraction spots in films with Ru spacers of 1.0 and 2.0 nm had some satellites, suggesting the possible formation of twins.

Cross-sectional high-angle annular dark-field scanning transmission electron microscopy (HAADF-STEM) images of the Fe-Pt/Ru(0.5)/Fe-Pt and Fe-Pt/Ru(1.0)/Fe-Pt films are shown in Fig. 3 along with the corresponding EDS maps and composition line profiles evaluated from the highlighted regions of interest. The grains in both films demonstrated the desired trilayer structure, which was featured with a curved interface. The bottom Fe-Pt tended to grow into nanograins with pronounced sphericity, which were then well wetted by Ru, forming such an unplanarity. According to EDS (Fig. 3, middle), there was a possibility of nonuniform chemical distribution and thickness of Ru along the curved interface with a decrease toward its edges. Across the center of the spacer (Fig. 3, bottom), Ru approached 35 and 55 at.% in the films with t_{sp} of 0.5 and 1.0 nm, respectively, while Fe and Pt occupied the rest content equally. However, the Ru content and thickness are prone to under- and over-estimation, respectively, because of the spacer curvature. Therefore, additional experiments were performed with continuous Fe-Pt(30)/Ru(t_{sp})/Fe-Pt(30) films deposited under the same conditions but without C segregant. In such an ideal case with a planar interface, the interdiffusion of layers was confirmed with Ru 55 at.%, Fe 20 at.% at t_{sp} = 0.5 nm and Ru 60 at.%, Fe 15 at.% at t_{sp} = 1.0 nm (Fig. S1 in Ref. [42]).

The alternating atomic layers of Fe and Pt were clearly visible in the bottom Fe-Pt (Fig. 3, top), indicating the formation of the $L1_0$ structure with a nice (001) texture in the out-of-plane direction. A similar feature was observed in the top Fe-Pt, but with some regions of deteriorated $L1_0$ order or texture (in-plane variants). Also note that despite similar nominal thicknesses designed for the top and bottom Fe-Pt layers, the top layer tended to be thinner due to wetting over the Ru spacer.

Fig. 4 shows the XRD patterns of Fe-Pt/Ru/Fe-Pt granular films with the inset depicting a change in the degree of $L1_0$ order (S) with increasing Ru thickness. In addition to the Fe-Pt (002) peak at $2\theta \approx 47.5°$, the (001) superlattice peak was observed at $2\theta \approx 23.5°$, indicating the $L1_0$ order in all films. The reference Fe-Pt film without Ru demonstrated a high degree of order, S = 0.86. When Ru was introduced, S started to decrease to 0.72 at t_{sp} = 2 nm. Note that here S is an effective degree of order that means an averaged value over the entire film, which may have different S in the top and bottom Fe-Pt layers following our previous study [15]. An insufficient misfit between the $L1_0$ Fe-Pt and fcc-Ru (1.3%) as well as the curved interface can result in a reduced S in the top Fe-Pt. A larger misfit is required to promote $L1_0$ ordering, *e.g.*, 10.3% in the case of MgO(100) substrate [43, 44].

B. Magnetic properties

The hysteresis loops of the Fe-Pt/Ru(t_{sp})/Fe-Pt films are shown in Fig. 5(a) for the OOP and IP directions. The reference Fe-Pt film (t_{sp} = 0 nm) had a typical square OOP loop with a high coercivity of 4.0 T, demonstrating a strong perpendicular magnetic anisotropy. When a thin Ru(0.5) spacer was introduced, the coercivity abruptly decreased to 1.7 T while the squareness of the OOP loop was preserved. The corresponding IP hysteresis loop was S-shaped near zero magnetic field, which could be attributed to some soft magnetic regions. With increasing Ru thickness, a step-like inflection appeared in the OOP loops close to the coercivity – the case of Ru(2.0) was the most illustrative. There were trends for the deterioration of OOP remanence and slight increase in coercivity shown in Figs. 5 (b) and (c), respectively. The S-shape of the IP hysteresis loops became more pronounced that can be quantified by the increasing IP remanence (Fig. 5(b)). The described transformations of the hysteresis loops could be caused by exchange coupling between the top and bottom Fe-Pt layers, the intensity of which was suppressed by increasing the Ru thickness. To verify this hypothesis and distinguish the magnetic properties of individual Fe-Pt layers, micromagnetic simulation was performed.

There are two different scenarios for the exchange coupling between Fe-Pt layers through the nonmagnetic Ru spacer. First, it can be a weakened direct exchange interaction enabled by a network of Fe atoms diffused into the Ru spacer (as in Ref. [45]). Another alternative is an indirect RKKY exchange interaction through metallic Ru [46, 47]. Although interdiffusion of the layers was observed, favoring the first scenario (Fig. 3 and Fig. S1), it is difficult to justify with certainty whether the concentration of Fe atoms is sufficient to realize such a cou-

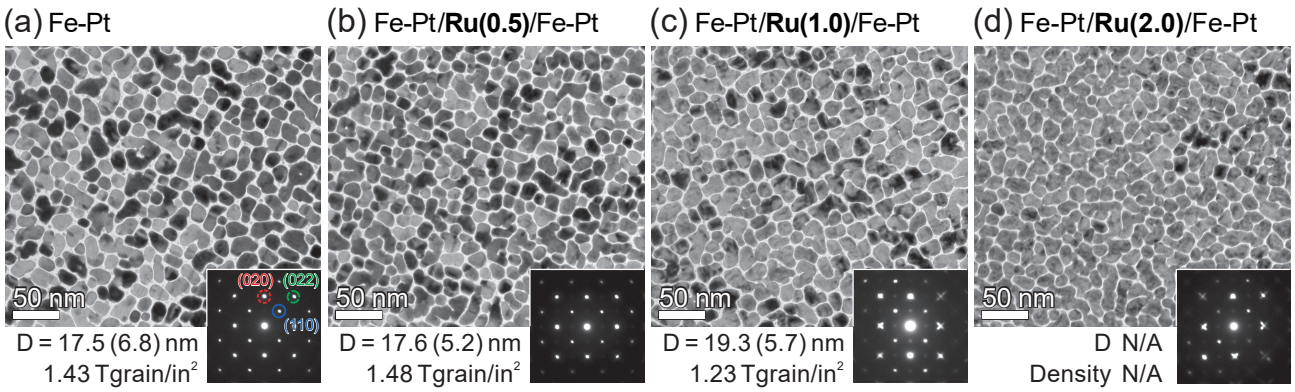

FIG. 2. Top view TEM images of the Fe-Pt/Ru/Fe-Pt films with different Ru thickness. The SAED patterns are shown in the insets. Where applicable, the average grain size (D) and number density are given at the bottom.

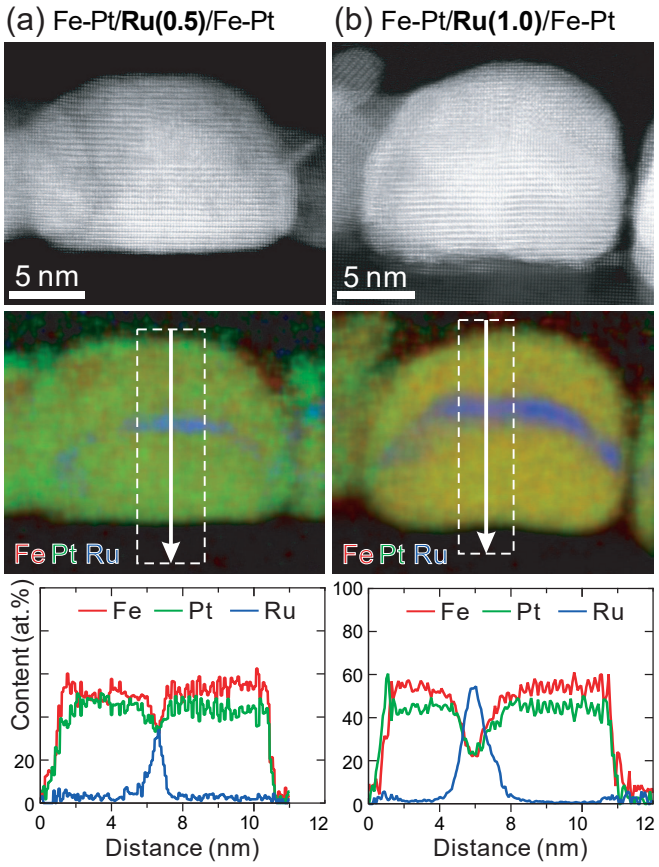

FIG. 3. Cross-sectional HAADF-STEM images, corresponding EDS maps, and composition line profiles of the Fe-Pt/Ru/Fe-Pt granular films with Ru thickness of (a) 0.5 nm and (b) 1.0 nm.

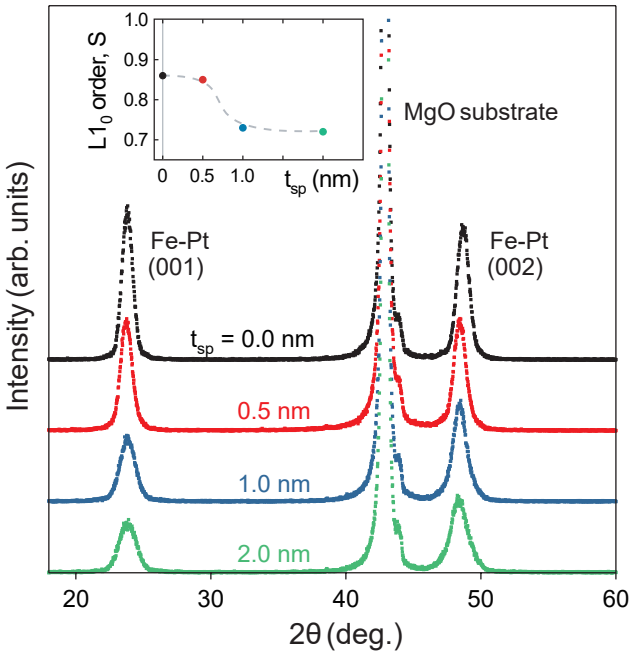

FIG. 4. XRD patterns of the Fe-Pt/Ru/Fe-Pt films with different Ru thickness (t_{sp}) and the effective degree of $L1_0$ order (S) as a function of t_{sp} (inset). Dashed line is a guide to the eye.

pling or not. An additional complexity arises from the curvature and potential nonuniformity of the Ru spacer described in the previous section. The up-to-date DFT calculations can clarify the origin of exchange coupling in the Fe-Pt/Ru/Fe-Pt granular media, either it is the RKKY interaction [49**?**] or direct exchange interaction via diffused Fe atoms [50].

However, both scenarios of exchange coupling would affect the hysteresis loops in a similar way. Therefore, we proceeded with a simplified micromagnetic model in which the Ru spacer is plain and weakly magnetic due to diffused Fe atoms (Fig. 6). The latter means that some saturation magnetization and exchange stiffness A_{sp} were prescribed to the spacer. They were varied in a grid search manner until the best correspondence between the simulated OOP demagnetization curves and experimental ones. Other varied parameters were the magnetic anisotropy constants K and volume fractions of in-plane variants V in the top and bottom Fe-Pt layers. The ini-

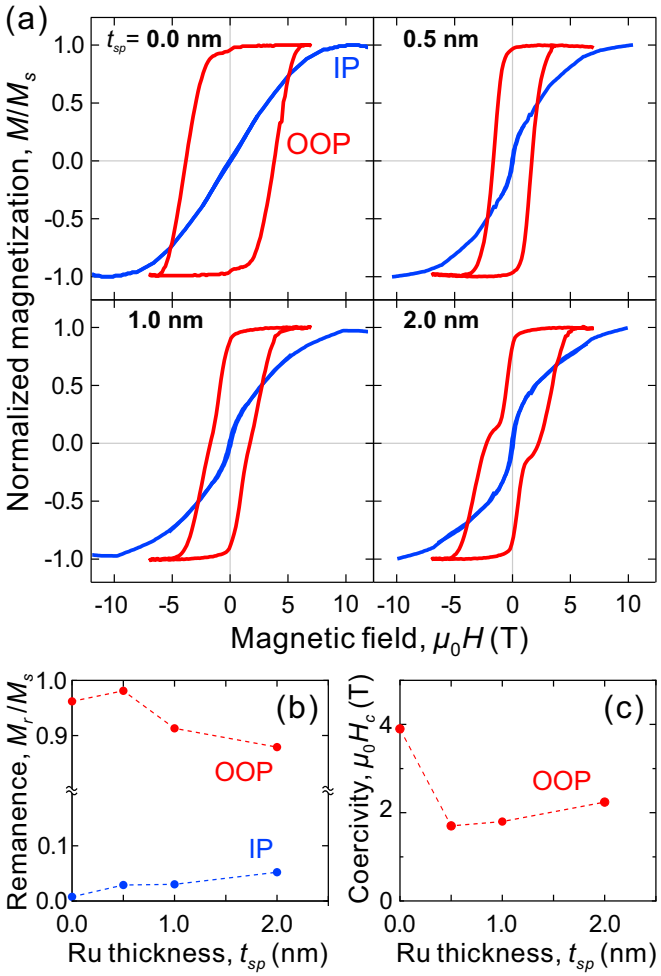

FIG. 5. (a) Out-of-plane (OOP) and in-plane (IP) hysteresis loops of Fe-Pt/Ru/Fe-Pt films with different Ru thickness (t_{sp}) measured at room temperature. (b) The normalized remanent magnetization and (c) coercivity as functions of Ru thickness.

tial parameters for the grid search were adopted from Ref. [15] in which the Fe-Pt(5)/Ru(3)/Fe-Pt(5) film with a thick spacer was studied. The saturation magnetization and exchange stiffness of both Fe-Pt layers were fixed to be 1.43 T and 10 pJ/m, respectively [15]. Despite the same nominal thicknesses of the Fe-Pt layers, the top Fe-Pt layer in the model was assumed to be 20% thinner than the bottom one. This was in agreement with TEM observations (Fig. 3) and with another feature - shifted up inflection points in the OOP loops with respect to the coercivities, as can be seen in Fig. 5(a).

The simulated OOP demagnetizations curves after the grid search are shown in Fig. 6(d). They described well the experimental demagnetization curves of Fe-Pt/Ru(t_{sp})/Fe-Pt films with t_{sp} of 0.5, 1.0, and 2.0 nm. The characteristics obtained for each layer are summarized in Table I. The top Fe-Pt layer had a significantly reduced magnetic anisotropy constant (lower $L1_0$ order) and a higher content of in-plane variants compared to the

TABLE I. Characteristics of each layer in Fe-Pt/Ru/Fe-Pt granular films, evaluated from the micromagnetic approximation in Fig. 6(d). K_u and V are the magnetic anisotropy constant (mean and standard deviation in parentheses) and volume fraction of in-plane variants in Fe-Pt layers, respectively. M_s and A_{sp} are the saturation magnetization and exchange stiffness of the Ru spacer with diffused Fe atoms.

Spacer			Bottom Fe-Pt		Top Fe-Pt	
t_{sp} (nm)	$\mu_0 M_s$ (T)	A_{sp} (pJ/m)	K_u (MJ/m^3)	V (vol.%)	K_u (MJ/m^3)	V (vol.%)
0.5	> 0.6	> 1.8	3.5 (0.45)	2	0.7 (0.1)	15
1.0	0.4	0.8	3.2 (0.45)	2	0.7 (0.1)	15
2.0	< 0.1	< 0.05	2.8 (0.45)	2	0.7 (0.1)	15

bottom Fe-Pt layer. The deteriorated quality of the top Fe-Pt layer was also evidenced in TEM (Fig. 3) and indirectly in XRD data (inset in Fig. 4). This was a detrimental consequence of depositing on the curved Ru spacer with insufficient interfacial stress for nice $L1_0$ (001) preferential growth.

The parameters of the top Fe-Pt layer did not vary with changing Ru thickness. The bottom Fe-Pt layer had a much higher magnetic anisotropy constant and only a slight trace of the in-plane variants. We observed that the magnetic anisotropy constant of the bottom Fe-Pt layer deteriorated with increasing Ru thickness, *i.e.*, it decreased from 3.5 to 2.7 MJ/m^3 when t_{sp} increased from 0.5 to 2.0 nm. This could be attributed to a deeper diffusion of Ru into Fe-Pt considering that Ru is detrimental to the magnetic anisotropy of Fe-Pt [16]. According to our simulations, the stack of magnetically soft/hard Fe-Pt layers was almost exchange-decoupled with the thick Ru spacer of 2 nm (Table I), resulting in such a pronounced step-like inflection in the OOP hysteresis loop (Fig. 6(d)). With decreasing Ru thickness, the exchange coupling between Fe-Pt layers became stronger, which was quantified by A_{sp} in Table I – A_{sp} of 1.8 pJ/m in Fe-Pt/Ru(0.5)/Fe-Pt was enough for a strong coupling with the eliminated $M(H)$ inflection.

The exchange coupling at room temperature was confirmed in Fe-Pt/Ru/Fe-Pt films with $t_{sp} < 2.0$ nm. As the next step, the magnetic properties of the films were examined with temperature. Fig. 7 shows the magnetization of Fe-Pt/Ru(t_{sp})/Fe-Pt films vs. temperature. The reference film without Ru spacer had the M-T curve typical for a uniform ferromagnetic material with T_c of 665 K. When the Ru layer was introduced, slight inflections were observed in the M-T curves of Fe-Pt/Ru(0.5)/Fe-Pt and Fe-Pt/Ru(1.0)/Fe-Pt films, which required the superposition of two Kuz'min equations with different Curie temperatures T_{c1} and T_{c2} for a better description. The lower T_{c1} was attributed to the top Fe-Pt layer due to its revealed defectiveness with lowered $L1_0$ order, while T_{c2} corresponded to the bottom Fe-Pt layer. Although it was hard to distinguish T_{c1} for films with t_{sp} of 0.5 and 1.0 nm due to experimental uncertainty, a distinct T_{c1} of the top Fe-Pt layer was observed for the exchange-decoupled Fe-

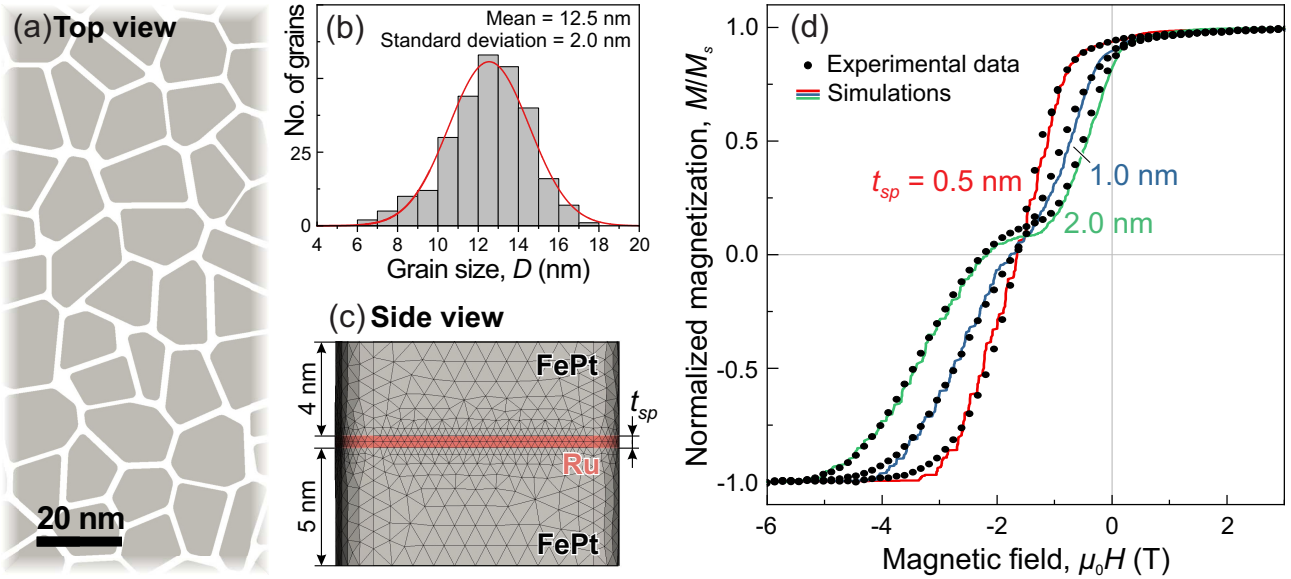

FIG. 6. (a) Top view fragment of the 240 × 240 nm^2 micromagnetic model of Fe-Pt/Ru/Fe-Pt granular film and (b) corresponding grain size distribution. (c) Side view on a meshed grain with highlighted Ru spacer which thickness (t_{sp}) was varied from 0.5 to 2.0 nm. (d) Experimental and simulated out-of-plane demagnetization curves of the films with different t_{sp}.

Pt/Ru(2.0)/Fe-Pt film with a value of about 400 K. This value can be considered as a reasonable landmark for T_{c1} in films with a thinner Ru spacer, assuming similar microstructural state of the top Fe-Pt layers. The T_{c2} of the bottom Fe-Pt layer in the exchange-decoupled Fe-Pt/Ru(2.0)/Fe-Pt film was of 655 K, that was close to T_c of the reference Fe-Pt film. Note that the interlayer exchange coupling should have no effect on T_{c2} given the same other factors, while T_{c1} could be enhanced to some extent by a strong coupling.

There are two factors that affect the Curie temperature of Fe-Pt and can result in low/high T_c layers. First, doping with Ru decreases the T_c of Fe-Pt [14, 15]. If there is a difference in the diffusion of Ru in the top and bottom Fe-Pt layers, distinct T_{c1} and T_{c2} can appear [15]. However, similar Ru diffusion profiles were observed in the top and bottom layers of the continuous Fe-Pt/Ru/Fe-Pt films (Fig. S1 in Ref. [42]). In addition, T_{c2} of the bottom layer in the Fe-Pt/Ru(2.0)/Fe-Pt film was close to T_c of the reference Fe-Pt film without Ru, indicating that Ru did not have a pronounced effect. The second factor is the degree of $L1_0$ order [51], which was distinct in the top and bottom Fe-Pt layers according to our experimental insights and simulations (indirectly via estimated K_u). This factor is supposed to be dominant for the low/high T_c observed in our study.

Fig. 8 shows the temperature dependencies of coercivity for Fe-Pt/Ru/Fe-Pt films with different Ru thicknesses. The reference Fe-Pt film without Ru exhibited a monotonous decrease in coercivity approaching 1.5 T, the current writing field threshold, at 565 K that can be considered as a writing temperature. The exchange-decoupled Fe-Pt/Ru(2.0)/Fe-Pt film possessed a lower

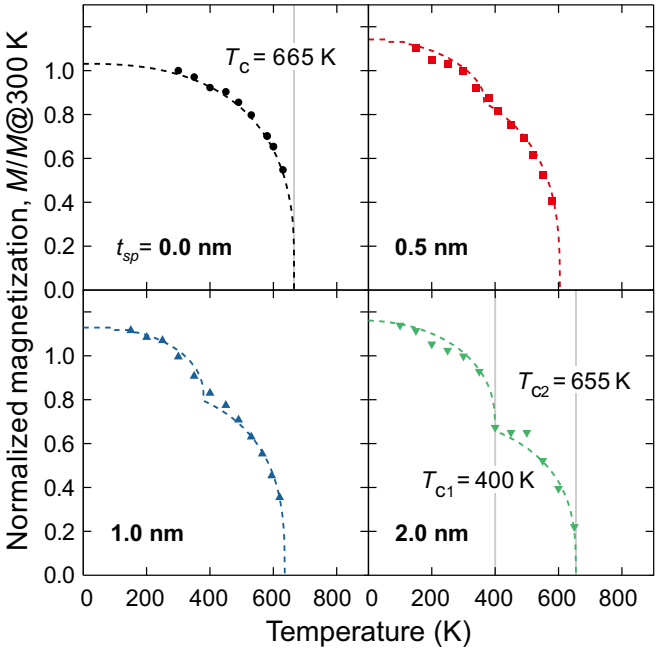

FIG. 7. Temperature dependence of magnetization for Fe-Pt/Ru/Fe-Pt films with different Ru thickness (t_{sp}). Dash lines correspond to the approximation by a superposition of two Kuz'min equations (one for t_{sp} = 0 nm) with distinct Curie temperatures (T_c).

writing temperature, while its coercivity dependence had a maximum at T_{c1} = 400 K. The magnetically softened top Fe-Pt layer magnetized oppositely to the bottom Fe-Pt layer in the vicinity of coercivity. Thus, the stray

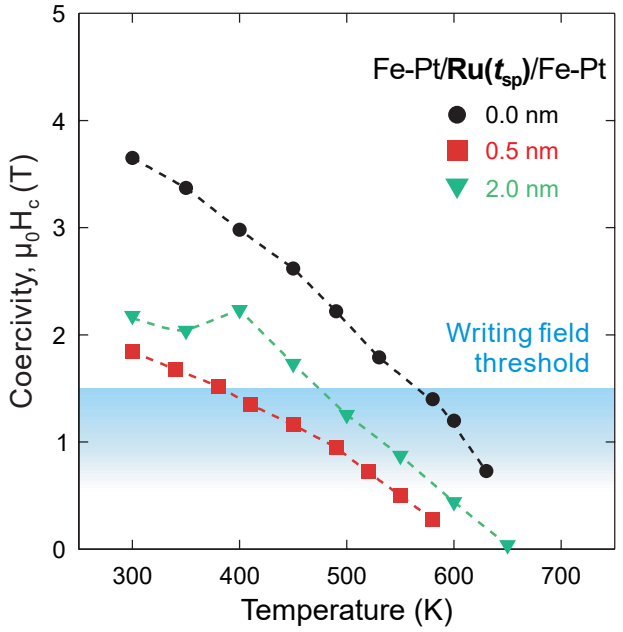

FIG. 8. Temperature dependence of coercivity for the Fe-Pt/Ru/Fe-Pt granular films with different Ru thickness (t_{sp}). The blue area indicates the magnetic field currently considered for the HAMR HDD write head [52].

field from the top layer reduces the coercivity of the bottom layer. Near T_{c1}, the magnetization of the top Fe-Pt layer abruptly decreases, as well as the corresponding stray field, thus increasing the coercivity of the bottom Fe-Pt layer and resulting in a local maximum. The coercivity dependence of the Fe-Pt/Ru(0.5)/Fe-Pt film with the strongest exchange coupling decreased without any anomaly, demonstrating a significantly reduced writing temperature of about 380 K. At the same time, its coercivity at room temperature was also notably decreased, so the next question was whether sufficient thermal stability was preserved or not.

The thermal stability of the exchange-coupled Fe-Pt/Ru/Fe-Pt films was depicted from the dynamic coercivity, whose time dependence follows the Sharrock equation [53]:

$$H_r(t) = H_{c_0}\left[1 - \left[\frac{k_B T}{E_b}\ln\left(\frac{f_0 t}{\ln 2}\right)\right]^{\frac{1}{n}}\right]. \qquad (2)$$

Such dynamic coercivity H_r can be interpreted as the reversed magnetic field at which half of the grains are switched during time t. Here H_{c_0} is a coercivity in the absence of thermal agitations, E_b is an effective energy barrier for magnetization switching at zero magnetic field, and f_0 is an attempt frequency [53]. The exponent n may vary depending on microstructural features, *e.g.*, grain misalignment, thicknesses of the ECC stack, etc. [53, 54]. For recording media including ECC, n of $1.4 - 1.5$ is usually considered [22, 55, 56]. The protocol for measuring $H_r(t)$ is described in Fig. 9(a) and (b) in details. Obtained $H_r(t)$ dependencies for the exchange-coupled Fe-Pt/Ru/Fe-Pt films and the reference Fe-Pt film are shown in Fig. 9(c). They were fitted using Eq. (2), providing values of the thermal stability coefficient summarized in Fig. 9(d). The reference Fe-Pt without Ru spacer had $K_u V/k_B T$ of about 260. The Fe-Pt/Ru(0.5)/Fe-Pt film with the strongest exchange coupling exhibited a lower $K_u V/k_B T$ of about 120, although it was still above the thermal stability threshold of 60. A bit better $K_u V/k_B T$ value of 160 was observed for the Fe-Pt/Ru(1.0)/Fe-Pt film.

Some critical notes should be emphasized in the end. First, the writing temperature derived from $H_c(T)$ (Fig. 8) may differ from that in a practical HAMR HDD with local heating and switching [57–59]. In addition, local switching is a dynamic process, so the interplay of exchange coupling and damping behavior in Fe-Pt/Ru/Fe-Pt is worth of further investigation via simulations [60, 61] and experimentally including elevated temperatures. The latter could be done with the all-optical time-resolved magneto-optical Kerr effect (TR-MOKE) [62], contributing to a discussion on how microstructural features affect the damping constant [61, 63, 64]. Second, although sufficient thermal stability was demonstrated in the case of exchange-coupled Fe-Pt/Ru(0.5)/Fe-Pt film, it was achieved for a relatively large grain size of 17.6 nm. To be of interest for practical application, the grain size of the developed media should be reduced to at least 7 nm. This should be feasible with further optimization of the sputtering conditions and exploration of other materials to be used as the spacer layer and segregant. For the latter, *h*-BN [65–68] and CrO_x [69, 70] can be potential candidates. The grain size reduction should be accompanied by an improvement in the microstructure of the top Fe-Pt layer. In particular, the K_u of this layer should be increased to maintain the thermal stability, while the appearance of in-plane variants should be suppressed. The realization of a flat interface between the top and bottom Fe-Pt layers would contribute to resolving the above problem.

IV. CONCLUSION

In this work, a series of Fe-Pt(4.5)/Ru(t_{sp})/Fe-Pt(4.5) films with t_{sp} = 0, 0.5, 1.0, 2.0 nm and 20 vol.% C segregant were fabricated by ultrahigh vacuum magnetron sputtering. The nanogranular microstructure was realized with the Fe-Pt/Ru/Fe-Pt trilayer interface in each grain. This interface had a pronounced curvature. The thin Ru spacer of 0.5 nm thickness did not affect the mean grain size, maintaining it at 17.6 nm, while further Ru thickening gradually deteriorated it, provoking grain coalescence. The nice $L1_0$ chemical ordering with (001) out-of-plane texture was confirmed for the bottom Fe-Pt layer. In contrast, the top Fe-Pt layer was more defective, showing some in-plane variants and reduced

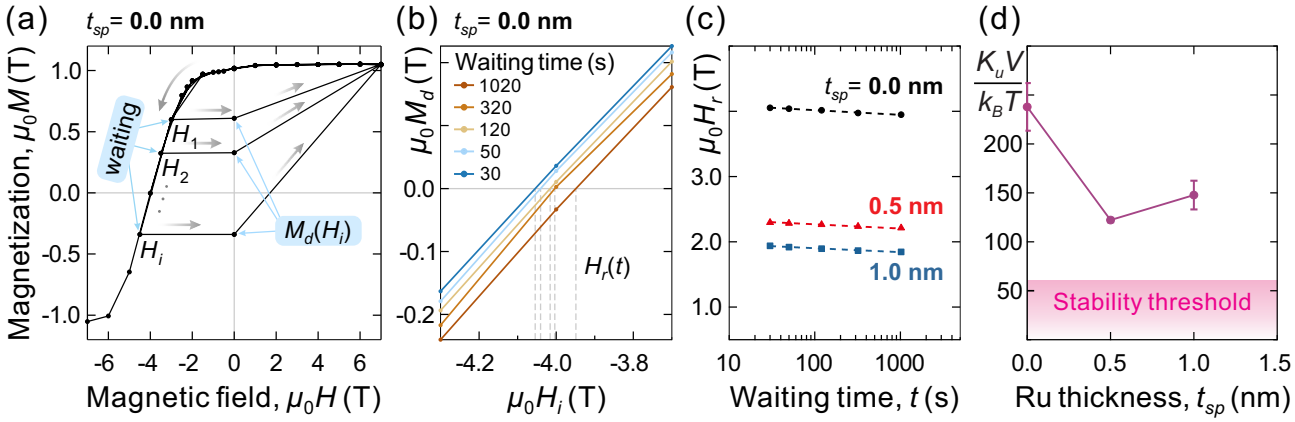

FIG. 9. (a) The protocol of measuring demagnetization remanence (M_d) as a function of increasing inverse applied magnetic field (H_i) performed for the reference Fe-Pt granular film (t_{sp} = 0 nm). After getting each M_d in the shown sequence, the film was exposed to magnetic saturation, then a higher H_i was applied with certain waiting time at this field. Finally, (b) the $M_d(H_i)$ plots at different waiting times allow to extract dynamic coercivities (H_r: H_i at which $M_d = 0$). (c) H_r as functions of waiting time for Fe-Pt/Ru/Fe-Pt granular films with different Ru thickness (t_{sp}) were analyzed using Eq. (2), giving (d) effective $K_u V/k_B T$.

$L1_0$ order, which resulted in softened magnetic properties of this layer. In addition, different Curie temperatures (T_c) were observed for the Fe-Pt/Ru/Fe-Pt films, which were attributed to the top (low T_c) and bottom (high T_c) Fe-Pt layers. The Fe-Pt layers were found to be exchange coupled when $t_{sp} < 2$ nm. In particular, the Fe-Pt/Ru(0.5)/Fe-Pt film with the strongest exchange coupling exhibited an inflectionless out-of-plane hysteresis loop, as well as nearly monotonic temperature dependencies of both magnetization and coercivity. Adjusting both the effective magnetic anisotropy and T_c of the Fe-Pt/Ru(0.5)/Fe-Pt film, we decreased its writing temperature to 380 K with a sufficient thermal stability coefficient $K_u V/k_B T = 120$. Thus, the feasibility of developing exchange-coupled HAMR media with a unique Fe-Pt/Ru/Fe-Pt trilayer nanogranular structure and the merit of controlling the writing temperature was demonstrated. The actual mechanism of exchange coupling and the effect of the curved interface on it are the subject of further studies, as well as the thorough microstructural optimization of such HAMR media toward a less defective the top Fe-Pt layer, smaller grain size, etc.

ACKNOWLEDGMENTS

The authors thank T. Hiroto, K. Yamaura, Y. Toyooka, T. Anzaki, Y. Mori, and A. Nakama (NIMS) for their contribution in conducting experiments. This work was supported in part by the JST-CREST (JPMJC22C3) and MEXT program: Data Creation and Utilization-Type Material Research and Development Project (JPMXP1122715503).

[1] B. Marchon, T. Pitchford, Y.-T. Hsia, and S. Gangopadhyay, The head-disk interface roadmap to an areal density of 4 Tbit/in^2, Adv. Tribol. 2013, 1–8 (2013).
[2] D. Weller, G. Parker, O. Mosendz, E. Champion, B. Stipe, X. Wang, T. Klemmer, G. Ju, and A. Ajan, A HAMR media technology roadmap to an areal density of 4 Tb/in^2, IEEE Trans. Magn. 50, 1–8 (2014).
[3] D. Weller, A. Moser, L. Folks, M. Best, W. Lee, M. Toney, M. Schwickert, J.-U. Thiele, and M. Doerner, High Ku materials approach to 100 Gbits/in^2, IEEE Trans. Magn. 36, 10–15 (2000).
[4] O. Ivanov, L. Solina, V. Demshina, and L. Magat, Determination of the anisotropy constant and saturation magnetization, and magnetic properties of powders of an iron-platinum alloy, Phys. Met. Metallog. 35, 81 (1973).
[5] G. Varvaro and F. Casoli, Ultra-High-Density Magnetic Recording: Storage Materials and Media Designs (Jenny Stanford Publishing, 2016).
[6] J. J. M. Ruigrok, Limits of conventional and thermallyassisted recording, J. Magn. Soc. Jpn. 25, 313–321 (2001).
[7] Y. K. Takahashi, Microstructure control for magnetic thin films with high functionality, J. Magn. Soc. Jpn. 46, 76–84 (2022).
[8] T. D. Trinh, S. Rajauria, R. Smith, E. Schreck, Q. Dai, and F. E. Talke, Temperature-induced near-field transducer failure in heat-assisted magnetic recording, IEEE Trans. Magn. 56, 1–4 (2020).
[9] B. X. Xu, Z. J. Liu, R. Ji, Y. T. Toh, J. F. Hu, J. M. Li, J. Zhang, K. D. Ye, and C. W. Chia, Thermal issues and their effects on heat-assisted magnetic recording system (invited), J. Appl. Phys. 111, 07B701 (2012).
[10] S. Bhargava and E. Yablonovitch, Lowering HAMR nearfield transducer temperature via inverse electromagnetic design, IEEE Trans. Magn. 51, 1–7 (2015).

[11] J. Zhang, R. Ji, J. Xu, J. Ng, B. Xu, S. Hu, H. Yuan, and S. Piramanayagam, Lubrication for heat-assisted magnetic recording media, IEEE Trans. Magn. 42, 2546–2548 (2006).

[12] M. Kaneko, K. Sueki, and Y. Kitamoto, Magnetic properties of $L1_0$ Fe-Ni-Pt films for heat assisted magnetic recording, J. Magn. Soc. Jpn. 30, 588–591 (2006).

[13] D. B. Xu, J. S. Chen, T. J. Zhou, and G. M. Chow, Effects of Mn doping on temperature-dependent magnetic properties of $L1_0$ FeMnPt, J. Appl. Phys. 109, 07B747 (2011).

[14] T. Ono, H. Nakata, T. Moriya, N. Kikuchi, S. Okamoto, O. Kitakami, and T. Shimatsu, Addition of Ru to $L1_0$-FePt thin film to lower Curie temperature, Appl. Phys. Exp. 9, 123002 (2016).

[15] P. Tozman, S. Isogami, I. Suzuki, A. Bolyachkin, H. Sepehri-Amin, S. Greaves, H. Suto, Y. Sasaki, T. Chang, Y. Kubota, P. Steiner, P. Huang, K. Hono, and Y. Takahashi, Dual-layer FePt-C granular media for multi-level heat-assisted magnetic recording, Acta Mater. 271, 119869 (2024).

[16] D. Suess, Multilayer exchange spring media for magnetic recording, Appl. Phys. Lett. 89, 113105 (2006).

[17] D. Suess, T. Schrefl, S. F¨ahler, M. Kirschner, G. Hrkac, F. Dorfbauer, and J. Fidler, Exchange spring media for perpendicular recording, Appl. Phys. Lett. 87, 012504 (2005).

[18] R. Victora and X. Shen, Composite media for perpendicular magnetic recording, IEEE Trans. Magn. 41, 537–542 (2005).

[19] Y. Sonobe, K. Tham, T. Umezawa, C. Takasu, J. Dumaya, and P. Leo, Effect of continuous layer in CGC perpendicular recording media, J. Magn. Magn. Mater. 303, 292–295 (2006).

[20] Y. K. Takahashi, K. Hono, S. Okamoto, and O. Kitakami, Magnetization reversal of FePt hard/soft stacked nanocomposite particle assembly, J. Appl. Phys. 100, 074305 (2006).

[21] T. Shimatsu, N. Asakura, Y. Inaba, K. Kudo, A. Sato, H. Muraoka, H. Aoi, S. Okamoto, and O. Kitakami, Thermal stability and switching field of hard/soft-stacked perpendicular media, J. Magn. Magn. Mater. 320, 3088–3091 (2008).

[22] J. Wang, H. Sepehri-Amin, Y. Takahashi, S. Okamoto, S. Kasai, J. Kim, T. Schrefl, and K. Hono, Magnetization reversal of FePt based exchange coupled composite media, Acta Mater. 111, 47–55 (2016).

[23] D. Suess and T. Schrefl, Breaking the thermally induced write error in heat assisted recording by using low and high T_c materials, Appl. Phys. Lett. 102, 162405 (2013).

[24] O. Muthsam, F. Slanovc, C. Vogler, and D. Suess, Improving the signal-to-noise ratio for heat-assisted magnetic recording by optimizing a high/low T_c bilayer structure, J. Appl. Phys. 126, 123907 (2019).

[25] K. Eason, H. T. Wang, M. R. Elidrissi, B. Xu, Z. Yuan, and K. S. Chan, Recording performance and comparison of graded-T_c and -K_u HAMR systems, IEEE Trans. Magn. 50, 107–113 (2014).

[26] N. Natekar, W. Tipcharoen, and R. Victora, Composite media with reduced write temperature for heat assisted magnetic recording, J. Magn. Magn. Mater. 486, 165253 (2019).

[27] N. Zhou, X. Xu, A. T. Hammack, B. C. Stipe, K. Gao, W. Scholz, and E. C. Gage, Plasmonic near-field transducer for heat-assisted magnetic recording, Nanophotonics 3, 141–155 (2014).

[28] O. Muthsam, C. Vogler, and D. Suess, Noise reduction in heat-assisted magnetic recording of bit-patterned media by optimizing a high/low T_c bilayer structure, J. Appl. Phys. 122, 213903 (2017).

[29] B. M. Lairson and B. M. Clemens, Enhanced magnetooptic Kerr rotation in epitaxial PtFe(001) and PtCo(001) thin films, Appl. Phys. Lett. 63, 1438–1440 (1993).

[30] J.-U. Thiele, L. Folks, M. F. Toney, and D. K. Weller, Perpendicular magnetic anisotropy and magnetic domain structure in sputtered epitaxial FePt (001) $L1_0$ films, J. Appl. Phys. 84, 5686–5692 (1998).

[31] I. Suzuki, J. Wang, Y. K. Takahashi, and K. Hono, Control of grain density in FePt-C granular thin films during initial growth, J. Magn. Magn. Mater. 500, 166418 (2020).

[32] C.-b. Rong, N. Poudyal, G. S. Chaubey, V. Nandwana, R. Skomski, Y. Q. Wu, M. J. Kramer, and J. P. Liu, Structural phase transition and ferromagnetism in monodisperse 3 nm FePt particles, J. Appl. Phys. 102, 043913 (2007).

[33] S. D. Granz and M. H. Kryder, Granular $L1_0$ FePt (001) thin films for heat assisted magnetic recording, J. Magn. Magn. Mater. 324, 287–294 (2012).

[34] E. Yang, D. E. Laughlin, and J.-G. Zhu, Correction of order parameter calculations for FePt perpendicular thin films, IEEE Trans. Magn. 48, 7–12 (2012).

[35] A. Perumal, Y. K. Takahashi, and K. Hono, $L1_0$ FePt–C nanogranular perpendicular anisotropy films with narrow size distribution, Appl. Phys. Exp. 1, 101301 (2008).

[36] E. Yang, D. E. Laughlin, and J.-G. Zhu, Buffer layers for highly ordered $L1_0$ FePt-oxide thin film granular media at reduced processing temperature, IEEE Trans. Magn. 46, 2446–2449 (2010).

[37] J. Christodoulides, P. Farber, M. Dannl, H. Okumura, G. Hadjipanaysi, V. Skumryev, A. Simopoulos, and D. Weller, Magnetic, structural and microstructural properties of FePt/M (M = C, BN) granular films, IEEE Trans. Magn. 37, 1292–1294 (2001).

[38] N. Kulesh, A. Bolyachkin, I. Suzuki, Y. Takahashi, H. Sepehri-Amin, and K. Hono, Data-driven optimization of FePt heat-assisted magnetic recording media accelerated by deep learning TEM image segmentation, Acta Mater. 255, 119039 (2023).

[39] M. D. Kuz'min, Shape of temperature dependence of spontaneous magnetization of ferromagnets: Quantitative analysis, Phys. Rev. Lett. 94, 107204 (2005).

[40] R. Chang, S. Li, M. V. Lubarda, B. Livshitz, and V. Lomakin, FastMag: Fast micromagnetic simulator for complex magnetic structures (invited), J. Appl. Phys. 109, 07D358 (2011).

[41] A. Bolyachkin, H. Sepehri-Amin, I. Suzuki, H. Tajiri, Y. Takahashi, K. Srinivasan, H. Ho, H. Yuan, T. Seki, A. Ajan, and K. Hono, Transmission electron microscopy image based micromagnetic simulations for optimizing nanostructure of FePt-X heat-assisted magnetic recording media, Acta Mater. 227, 117744 (2022).

[42] See Supplemental Material at [URL will be inserted by publisher], for details about the cross-sectional HAADF-STEM images of Fe-Pt/Ru/Fe-Pt continuous films and for out-of-plane hysteresis loops of these films with various temperatures.

[43] M. Futamoto, M. Nakamura, T. Shimizu, M. Ohtake, and N. Inaba, Influence of stress and strain on $L1_0$-ordered phase formation in FePt thin film, IEEE Trans. Magn. 54, 1–4 (2018).

[44] I. Suzuki, S. Kubo, H. Sepehri-Amin, and Y. K. Takahashi, Dependence of the growth mode in epitaxial FePt $L1_0$ films on surface free energy, ACS Appl. Mater. Interfaces 13, 16620–16627 (2021).

[45] R. F. L. Evans, Q. Coopman, S. Devos, W. J. Fan, O. Hovorka, and R. W. Chantrell, Atomistic calculation of the thickness and temperature dependence of exchange coupling through a dilute magnetic oxide, J. Phys. D: Appl. Phys. 47, 502001 (2014).

[46] J. Jiang, N. Tezuka, and K. Inomata, Exchange coupling between FePt and Fe through Ru interlayer, J. Appl. Phys. 98, 063902 (2005).

[47] J. Jiang, N. Tezuka, and K. Inomata, Indirect exchange spring between FePt and Fe with a Ru interlayer, J. Magn. Magn. Mater. 302, 40–46 (2006).

[48] T. Nomoto, T. Koretsune, and R. Arita, Formation mechanism of the helical Q structure in Gd-based skyrmion materials, Phys. Rev. Lett. 125, 117204 (2020).

[49] S. Liang, R. Chen, Q. Cui, Y. Zhou, F. Pan, H. Yang, and C. Song, Ruderman–Kittel–Kasuya–Yosida-type interlayer Dzyaloshinskii–Moriya interaction in synthetic magnets, Nano Letters 23, 8690 (2023).

[50] T. Fukushima, H. Akai, T. Chikyow, and H. Kino, Automatic exhaustive calculations of large material space by Korringa-Kohn-Rostoker coherent potential approximation method applied to equiatomic quaternary high entropy alloys, Phys. Rev. Mater. 6, 023802 (2022).

[51] D. Isurugi, T. Saito, S. Kaneko, K. K. Tham, T. Ogawa, and S. Saito, Evaluation of blocking temperature and its distribution for $L1_0$-type FePt granular films, J. J. Appl. Phys. 62, 045503 (2023).

[52] Z. Li, D. Wei, and F. Wei, Micromagnetic modeling for heat-assisted magnetic recording, J. Magn. Magn. Mater. 320, 3108–3112 (2008).

[53] M. Sharrock, Recent advances in metal particulate recording media: toward the ultimate particle, IEEE Trans. Magn. 36, 2420–2425 (2000).

[54] D. Suess, S. Eder, J. Lee, R. Dittrich, J. Fidler, J. W. Harrell, T. Schrefl, G. Hrkac, M. Schabes, N. Supper, and A. Berger, Reliability of Sharrocks equation for exchange spring bilayers, Phys. Rev. B 75, 174430 (2007).

[55] J. Harrell, Orientation dependence of the dynamic coercivity of Stoner-Wohlfarth particles, IEEE Trans. Magn. 37, 533–537 (2001).

[56] S. Okamoto, Experimental approaches for micromagnetic coercivity analysis of advanced permanent magnet materials, Sci. Technol. Adv. 22, 124–134 (2021).

[57] P. K. Venuthurumilli, Z. Zeng, and X. Xu, Inverse design of near-field transducer for heat-assisted magnetic recording using topology optimization, IEEE Trans. Magn. 57, 1–6 (2021).

[58] N. A. Natekar, E. Roddick, and R. M. Brockie, Interplay of the thermal and magnetic fields in HAMR, IEEE. Trans. Magn. 58, 1–8 (2022).

[59] F. Akagi and N. Matsushima, Relationship between temperature rise and thermal conductivity in a magnetic medium during heated dot magnetic recording, J. J. Appl. Phys. 62, SB1001 (2022).

[60] R.-V. Ababei, M. O. A. Ellis, R. F. L. Evans, and R. W. Chantrell, Anomalous damping dependence of the switching time in Fe/FePt bilayer recording media, Phys. Rev. B 99, 024427 (2019).

[61] C. Liu, K. Srinivasan, A. Ajan, E. McCollum, A. Kalitsov, V. Kalappattil, and M. Wu, Ferromagnetic resonance in FePt thin films at elevated temperatures, J. Magn. Magn. Mater. 563, 169988 (2022).

[62] Y. Sasaki, I. Suzuki, R. Mandal, S. Kasai, and Y. K. Takahashi, Thermal modulation of magnetization dynamics in nanometer-thick $L1_0$-FePt nanogranular and continuous films for high-density magnetic recording media, ACS Appl. Nano Mater. 6, 5901–5908 (2023).

[63] D. Richardson, S. Katz, J. Wang, Y. K. Takahashi, K. Srinivasan, A. Kalitsov, K. Hono, A. Ajan, and M. Wu, Near-T_c ferromagnetic resonance and damping in FePt-based heat-assisted magnetic recording media, Rhys. Rev. Appl. 10, 054046 (2018).

[64] I. Kurniawan, Y. Miura, G. Xing, T. Tadano, and K. Hono, Theoretical study of the effect of lattice dynamics on the damping constant of FePt at finite temperature, Phys. Rev. B 108, 094426 (2023).

[65] C. Xu, B. Zhou, T. Du, B. S. D. C. S. Varaprasad, D. E. Laughlin, and J.-G. J. Zhu, Understanding the growth of high-aspect-ratio grains in granular $L1_0$-FePt thin-film magnetic media, APL Mater 10, 051105 (2022).

[66] C. Xu, B. S. D. C. S. Varaprasad, D. E. Laughlin, and J.-G. Zhu, Fabrication of 16 nm Thick Granular $L1_0$ FePt-hBN Thin Film Media, IEEE Trans. Magn. 59, 1–5 (2023).

[67] B. S. D. C. S. Varaprasad, C. Xu, M.-H. Huang, D. E. Laughlin, and J.-G. Zhu, FePt–BN granular HAMR media with high grain aspect ratio and high $L1_0$ ordering on corning LotusTM NXT glass, AIP Adv 13, 035002 (2023).

[68] C. Xu, B. S. D. C. S. Varaprasad, D. E. Laughlin, and J.-G. Zhu, Bias sputtering of granular $L1_0$-FePt films with hexagonal boron nitride grain boundaries, Sci. Rep 13, 11087 (2023).

[69] T. Shiroyama, B. S. D. C. S. Varaprasad, Y. K. Takahashi, and K. Hono, Microstructure and Magnetic Properties of FePt–Cr_2O_3 Films, IEEE Trans. Magn. 50, 1–4 (2014).

[70] I. Suzuki, T. Abe, H. Sepehri-Amin, K. Hono, and Y. Takahashi, Microstructure evolution in FePt-Cr_2O_3 granular thin films, J. Magn. Magn. Mater 579, 170874 (2023).